A Time-Shift Model for OFDM Radar

David Frederic Crouse
Naval Research Laboratory
4555 Overlook Ave., SW
Washington DC 20375
E-Mail: david.crouse@nrl.navy.mil

***Abstract*—Active and passive detection using CP-OFDM modulated signals traditionally assume that targets do not move significantly during the entire observation period. In this paper, a "time-shift" model that compensates for the motion of targets between pulses during the observation period is introduced. Matched filtering based upon this model can be efficiently performed using a combination of the chirp-z transform and the fast Fourier transform algorithms. The resulting delay-Doppler plots are less "smeary" in the range axis than plots generated when using the traditional techniques over extended observation intervals, allowing better resolution of closely spaced targets.**

I. Introduction

RECENT work has noted the merits of using signals modulated with Orthogonal Frequency Division Multiplexing (OFDM) in radar applications. In [19], OFDM was utilized in the form of a Multifrequency Complementary Phase Coded (MCPC) signal, where it was shown to exhibit more efficient spectral usage and lower sidelobes in the ambiguity function than traditional techniques. Additionally, in [12], it was noted that OFDM signals do not experience range-Doppler coupling. One of the most appealing properties of OFDM waveforms is their ability to be used simultaneously for communications and radar. Aspects of radar-based communication, such as the range and throughput, have been explicitly studied by some researchers [18], [24]. However, most research on OFDM signals has been from the communications community.

Most countries have now transitioned to digital television and radio broadcasting to some extent or utilize forms of long-range wireless networking, and in most cases, the standards used are based on a form of OFDM [21], [26], [25], as shown in Table I.[1] The wide proliferation of OFDM broadcasters worldwide and the ease with which an individual could erect a new television or radio station, or networking tower without raising suspicion have spawned interest in utilizing OFDM signals for passive detection. The suitability of the signals for detection varies based upon the specific standard.

Range migration, also known as range walk, is a "smearing" that occurs in radar, as well as in general signal processing [6], when performing matched filtering without compensating for the motion of a target during the observation period. Range walk is particularly problematic when using long integration times for detection. Without compensation, it limits the coherent integration gain, lowering the probability of detecting weak targets [7], [20], and is also a problem with incoherent integration [2].

This paper derives a time-shift model that addresses the range-walk problem and that can be efficiently implemented for OFDM signals, among others. A lot of work regarding range migration compensation has been done for Synthetic Aperture Radar (SAR) [16] and in wideband signal processing [17]. Whereas the wideband model in [17] relies on time-domain processing, the technique in this paper processes the data in the Fourier domain, performing interpolation when non-integer shifts are needed. The algorithm coming from the time-shift model is conceptually similar to the approach outlined in the expired patent [13], which implements a keystone transform using FFTs and a "special" (not necessarily computationally efficient) Discrete Fourier Transform (DFT). Note that range migration is not necessarily a negative effect, as it can be used to eliminate clutter in a migrating target indicator detector [8].

The OFDM-modulated signals being received are assumed to have been modulated with a cyclic prefix (CP-OFDM), making this work relevant for passive detection utilizing most OFDM-based broadcast standards, with a notable exception being the DTMB standard, which is the digital television standard in China.[2] However, not all CP-OFDM codes are equally suited for the type of low-complexity radar processing considered here. As was the case in [5], each OFDM symbol is treated as a "pulse" and it is assumed that the maximum delay of a return from the target compared to the direct-path return from the nearest receiver is less than the duration of the cyclic prefix, which occupies the interval between pulses. Since error correction codes are used in all digital broadcast standards, the digital signal is assumed to have been correctly decoded and properly synchronized.

In Section II, the ideal models of the transmitted and received signals as well as the time-shift approximation, which is the subject of this paper, are presented. In Section III expressions for estimating the channel taps and performing matched filtering using the new model are presented. Section IV discusses the discrete-time implementation of the matched filters. In Section V, the delay-Doppler plots created using each of the methods in scenarios involving synthetically gen-

[1] A notable exception is the digital television standard in the United States, Canada, Mexico and South Korea, the Advanced Television Systems Committee (ATSC) standard [1], which does not use OFDM.

[2] The DTMB standard puts pseudonoise in the guard interval between symbols rather than using a cyclic prefix. It has been claimed that the use of pseudonoise facilitates synchronization between the transmitter and the receivers. [23]

Acronym	Meaning	Notable Areas Where Used	Specifications
Major Digital Television Standards			
ISDB-T	Integrated Services Digital Broadcasting - Terrestrial	Japan, most of South America	[3]
DTMB DMB-T/H	Digital Terrestrial Multimedia Broadcast Digital Multimedia Broadcast - Terrestrial/Handheld	China, Hong Kong, Madagascar	[23]
DVB-T DVB-T2	Digital Video Broadcasting - Terrestrial	Australia, Europe, India, Iran, Russia, most of Africa and the Middle East	[11], [10]
Major Digital Radio Standards			
DAB	Digital Audio Broadcasting	Australia, China, Europe, Russia	[9]
HDRadio	Hybrid Digital Radio	United States	[14]
Major Networking Standards			
WiMAX	Worldwide Interoperability for Microwave Access	150 countries	[15]

TABLE I: Major long-range broadcast standards around the world that use forms of OFDM modulation.

erated digital audio and video signals are compared, and the results are summarized in Section VI.

II. The Generalized Model

A. The Transmitted Signal Model

The transmitted signal model is the same as that used in [5], which is standard for OFDM signals. Let $N+1$ be the number of subcarriers (discrete, orthogonal frequencies) used in the OFDM symbols. Under the assumption that N is an even integer,[3] the ith baseband modulated symbol in the continuous domain, generated by multiplexing complex values onto orthogonal subcarriers,[4] is given by

$$x_i(t) = \sum_{m=-\frac{N}{2}}^{\frac{N}{2}} s_i[m] e^{j2\pi m \Delta f t} q(t), \tag{1}$$

where $s_i[m]$ is the symbol being sent in the ith block, Δf is the spacing (in frequency) between subcarriers, and

$$q(t) = \begin{cases} 1 & t \in [-T_{cp}, T_s], \\ 0 & \text{otherwise.} \end{cases} \tag{2}$$

The total duration of the block is $T_b = T_s + T_{cp}$, where T_s is the information-carrying modulated symbol and T_{cp} is a cyclic prefix such that $q(t) = q(t + T_s)$ for $t \in [0, T_{cp}]$. The cyclic prefix occupies a region between symbols known as the "guard interval." The guard interval is assumed to be greater than or equal to the length of the channel response so as to avoid inter-symbol interference (ISI). The frequencies are orthogonal, because $\Delta f = \frac{1}{T_s}$. The baseband broadcast signal is given by the concatenation of all of the symbols over time,

$$x(t) = \sum_{i=-\infty}^{\infty} x_i(t - iT_b). \tag{3}$$

The passband signal is given by

$$x_{\text{pass}}(t) = \Re\left\{ e^{j2\pi f_c t} x(t) \right\}, \tag{4}$$

where f_c is the center carrier frequency.

B. The Target Model

1) The Full Model: The received signal at a particular antenna should consist of a direct-path contribution from each transmitter (assuming a clear line of sight) as well as from reflections off stationary objects and the targets. It is assumed that each subcarrier experiences the same complex attenuation. Under the standard non-relativistic Doppler model, the received passband signal at time t of a reflection from a single target traveling at a constant range rate is

$$y_{\text{pass}}(t) = \Re\left\{ e^{j2\pi f_c (t - \tau_0 - a_d t)} A_0 x(t - \tau_0 - a_d t) \right\}, \tag{5}$$

where τ_0 is the bistatic delay of the return from the target at time $t = 0$, the term $a_d t$ expresses how the bistatic delay has changed over time where $a_d = v_d/c$ is the ratio[5] of the range rate v_d of the target to the speed of light c, and A_0 is the complex attenuation of the received signal.

Thus, the complex baseband signal consisting of N_T reflections (the number of discrete scatterers modeled) is

$$y(t) = \sum_{p=0}^{N_T - 1} e^{-j2\pi f_c (\tau_p + a_p t)} A_p x(t - \tau_p - a_p t), \tag{6}$$

where τ_p is the bistatic delay from the pth return at time 0, A_p is the complex attenuation of the signal, and a_p is the corresponding Doppler shift.

The full model under the assumption of uniform complex attenuation across subcarriers is the model used to generate data in the simulation section. Unfortunately, this model is too computationally demanding to perform matched filtering in real time on a regular computer. For that reason, the time-shift approximation is introduced.

2) The Time-Shift Model: Reference [5] noted that it is not unusual to use a large number of blocks for detection in passive scenarios (on the order of 1 s). Unfortunately, the traditional phase-shift model of [5] does not compensate for the motion of the target during the observation interval. During that time, the targets can be expected to have moved considerably. The time-shift model partially accounts for this motion. The bistatic range shall be considered constant for individual blocks, but will be allowed to change between

[3] All of the broadcast standards in Table I have chosen N to be an even integer. Though the concepts presented here apply if the center carrier frequency does not correspond to one of the subcarriers, which occurs when N is not an integer, the notation becomes cumbersome and has consequently been omitted.

[4] The numbering of the subcarriers about the center carrier frequency is consistent with the notation used in multiple standards. Generally, the DC subcarrier is not used. A different organization of the subcarriers could be chosen without changing the results in the paper.

[5] This ratio is the Doppler shift.

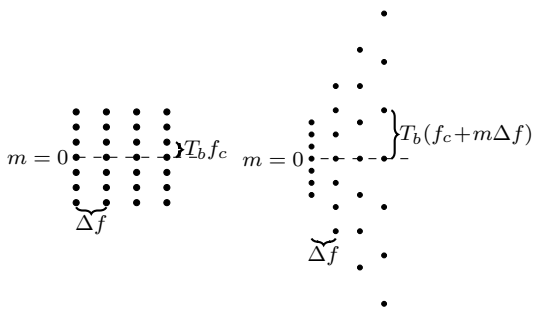

(a) The Phase-Shift Model (b) The Time-Shift Model

Fig. 1: The signal model for the channel taps with respect to the delay and Doppler components of the target returns is that of planar waves impinging upon a uniform rectangular array, in the traditional phase-shift model and that of waves impinging upon a nonuniform (keystone) array in the time-shift model.

blocks. Under this assumption, the model for the ith received symbol becomes, for $t \in \{-T_{cp}, T_s\}$,

$$y^{(i)}(t) = \sum_{p=0}^{N_T-1} A_p e^{-j2\pi f_c(\tau_p + a_p i T_b)} x_i(t - \tau_p - a_p i T_b). \quad (7)$$

III. The Data Processing for Estimation

A. The Virtual Antenna Array

Reference [5] demonstrated how the OFDM channel estimates can be used as a virtual rectangular array for estimating delay and Doppler. The channel tap estimates that form the virtual array for the time shift model are given by

$$h_m^{(i)} \triangleq s_i[m]^* \int_0^{T_s} e^{-j2\pi m\Delta f t} y^{(i)}(t) dt \quad (8a)$$

$$= \sum_{p=0}^{N_T-1} A_p e^{-j2\pi f_c(\tau_p + a_p i T_b)} \sum_{n=-\frac{N}{2}}^{\frac{N}{2}} s_i[m]^* s_i[n] e^{-j2\pi n\Delta f(\tau_p + a_p i T_b)} \int_0^{T_s} e^{-j2\pi(m-n)\Delta f t} dt. \quad (8b)$$

Since the integral in (8b) is over an entire period, when $n \neq m$, every positive value of the argument as a function of t can always be cancelled by one with a negative value, and the integral must be zero. On the other hand, if $m = n$, then the exponential is 1, and the integral is equal to T_s. All together, the solution reduces to:

$$h_m^{(i)} = T_s \sum_{p=0}^{N_T-1} A_p |s_i[m]|^2 e^{-j2\pi(\tau_p(f_c + m\Delta f) + a_p i T_b(f_c + m\Delta f))}, \quad (9)$$

which is equivalent to an expression for the received signal from an antenna located at $(\Delta f, T_b(f_c + m\Delta f))$ in a planar phased array having N_T impinging waves. However, unlike in [5], the spacing of the virtual elements no longer forms a uniform rectangle. Figure 1 illustrates how the layout of the elements in the virtual arrays differs between models.

B. The Matched Filter Receiver

A matched filter receiver correlates a waveform given a specific Doppler shift and delay to the received signal over N_B blocks. The matched filter for delay τ and Doppler shift a_d under the traditional phase-shift model is typically given by

$$z_d(\tau) = \int_0^{N_B T_b} e^{j2\pi a_d f_c t} x^*(t - \tau) y(t) dt. \quad (10)$$

Unfortunately, with integration periods on the order of one second not being unusual for passive detection, the motion of the target during the interval becomes significant. By treating each block as a "pulse" and omitting the cyclic prefix, so as to avoid ISI, the matched filter for the time-shift model becomes

$$z_d(\tau) = \sum_{i=0}^{N_B-1} \int_0^{T_s} e^{j2\pi f_c(\tau_p + a_p i T_b)} x_i^*(t - \tau_p - a_p i T_b) y^{(i)}(t) dt \quad (11a)$$

$$= \sum_{i=0}^{N_B-1} e^{j2\pi f_c(\tau_p + a_p i T_b)} \sum_{m=-\frac{N}{2}}^{\frac{N}{2}} e^{j2\pi m\Delta f(\tau_p + a_p i T_b)} h_m^{(i)}. \quad (11b)$$

IV. Discrete-Time Implementation of the Filters

In the discrete domain, the durations, T_s and T_{cp}, of the modulated symbol and the cyclic prefix are chosen to be multiples of the sampling period, T_0; that is, $T_s = N_s T_0$ and $T_{cp} = N_{cp} T_0$. Additionally, it is assumed that $N_s > N$. In discussing the practical implementation of the discrete-time filters, the discrete Fourier transform (DFT) and the chirp-z Transform (CZT) will be used. The CZT of the length N_s sequence z is defined to be

$$\mathrm{CZ}[k] \triangleq e^{j2\pi\omega_0} \sum_{m=0}^{N_s-1} e^{-j\frac{2\pi}{N_s} km\alpha} z[m] \quad \forall k = \{0, \ldots, N_s - 1\}, \quad (12)$$

where the constant α can be any complex number and ω_0 defines an initial phase shift. The CZT algorithm can be efficiently computed using DFTs, as described in [22]. The CZT has found use in decoding CP-OFDM modulated signals for passive radar when using technology having a sampling rate [4] that does not match the sampling rate assumed when designing the signal such that the OFDM subcarriers truly are orthogonal. This situation can occur in radars not explicitly designed for passive reception of digital broadcast signals.

A. Calculating the Channel Estimates

In the discrete-time domain, the channel tap estimate of (8a) becomes

$$h_m^{(i)} = \frac{s_i^*[m]}{N_s} \sum_{k=0}^{N_s-1} e^{-j\frac{2\pi}{N_s} km} y^{(i)}[k]. \quad (13)$$

For each block (each value of i), one can evaluate the channel tap estimates for all $m \in \{-\frac{N}{2}, \ldots, 0, \ldots, \frac{N}{2}\}$ in two steps

$$|z_d(\tau)| = \left| \sum_{n=0}^{N} e^{-j2\pi \frac{n\tilde{\tau}}{M_1 N_s}} \sum_{k=0}^{N_F-1} \left(e^{-j2\pi \frac{\tilde{v}_d}{M_2 N_B}\left(\frac{kT_f}{T_b}\right)\alpha_n} \sum_{i=0}^{N_B-1} e^{-j2\pi \frac{i\tilde{v}_d}{M_2 N_B}\alpha_n} h^{(i)}_{n-\frac{N}{2}}(k) \right) \right| \tag{20}$$

$$|z_d(\tau)| = \left| \sum_{n=0}^{N} e^{-j2\pi \frac{n\tilde{\tau}}{M_1 N_s}} \sum_{k=0}^{N_F-1} e^{-j2\pi N_A \left(\frac{kT_f}{T_b}\right)\alpha_n} \left(e^{-j2\pi \frac{\tilde{v}_d}{M_2 N_B}\left(\frac{kT_f}{T_b}\right)\alpha_n} \sum_{i=0}^{N_B-1} e^{-j2\pi \frac{i\tilde{v}_d}{M_2 N_B}\alpha_n} \left(e^{-j2\pi N_A i\alpha_n} h^{(i)}_{n-\frac{N}{2}}(k) \right) \right) \right| \tag{21}$$

as

$$\mathbf{t} = \mathrm{DFT}\left(\mathbf{y}^{(i)}\right), \tag{14}$$

$$\mathbf{h}^{(i)} = \frac{1}{N_s}\mathbf{s}_i^* \circ \mathrm{circshift}\left(\mathbf{t}, N/2\right), \tag{15}$$

where the vectors $\mathbf{s}_i$ and $\mathbf{h}^{(i)}$ are defined to be

$$\mathbf{s}_i \triangleq \left[s_i\left[-N/2\right], \ldots, s_i[0], \ldots, s_i\left[N/2\right]\right]', \tag{16}$$

$$\mathbf{h}^{(i)} \triangleq \left[h^{(i)}_{-N/2}, \ldots, h^{(i)}_0, \ldots, h^{(i)}_{N/2}\right]', \tag{17}$$

and $\mathbf{t}$ is a temporary vector of length N_s. The length N_s vector $\mathbf{y}^{(i)}$ consists of the signal samples received during block i. The circular shift operation in (15) means that the elements in the length N_s vector $\mathbf{t}$ are rotated such that an element at position k is moved to position $(k + N/2) \mod (N_s)$. Only the first $N+1$ elements of $\mathbf{h}^{(i)}$ provide useful information, since they correspond to values of m from $-N/2$ to $N/2$.

B. Calculating the Correlator Outputs

When using the time-shift model of (11b) generalized over the coherent combination of multiple frames (collections of N_B blocks separated by an empty region), the matched filter becomes

$$z_d(\tau) = \sum_{k=0}^{N_F-1} \sum_{m=-\frac{N}{2}}^{\frac{N}{2}} \sum_{i=0}^{N_B-1} e^{j2\pi(f_c+m\Delta f)(\tau+a_d(kT_f+iT_b))} h^{(i)}_m(k) \tag{18a}$$

$$= e^{j2\pi f_c \tau} \sum_{k=0}^{N_F-1} \sum_{m=-\frac{N}{2}}^{\frac{N}{2}} e^{j2\pi m\Delta f \tau} \times \sum_{i=0}^{N_B-1} e^{j2\pi(f_c+m\Delta f)a_d(iT_b+kT_f)} h^{(i)}_m(k), \tag{18b}$$

where N_F is the number of frames, T_f is the duration of a frame, and τ is the delay of the signal reflected from the target with respect to the direct path signal. Let M_1 and M_2 be positive integers greater than or equal to one. Their role will only be for interpolating extra points in an FFT (effectively zero padding). If one wishes to operate at the Rayleigh resolution, set them both to unity. Remembering that $a_d = v_d/c$, where c is the speed of light, the following substitutions can be made

$$\tau = -\frac{\tilde{\tau}T_0}{M_1} \quad v_d = -\frac{\tilde{v}_d}{M_2 N_B\left(\frac{f_c T_b}{c}\right)} \quad m = n - \frac{N}{2}, \tag{19}$$

resulting in Equation 20, where

$$\alpha_n \triangleq \frac{f_c + (n - N/2)\Delta f}{f_c}. \tag{22}$$

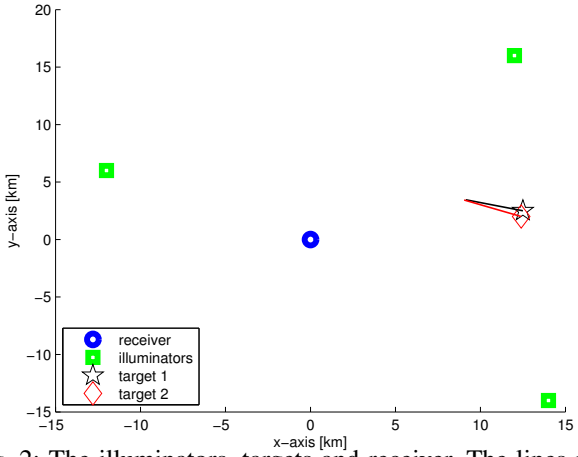

Fig. 2: The illuminators, targets and receiver. The lines represent the direction in which the targets travel; the shapes mark where the tracks begin.

The innermost sum of (20) can be evaluated across all Doppler shifts for each frame and bistatic range using the CZT. However, due to the definition of the CZT, this formulation only allows for *negative* velocities to have their range migration corrected. In reality, one does not want to evaluate the CZT at the discrete bistatic range rates $\tilde{v}_d$ (which map to negative continuous bistatic range rates), but rather at $\tilde{v}_d + N_A\,(M_s N_B)$, where $N_A = -1/2$. This gives us a range of velocities of $\tilde{v}_b = -\frac{M_2 N_B}{2} + 1$ to $\tilde{v}_b = \frac{M_2 N_B}{2}$. Thus, the desired transform is actually that given in (21). Consequently, for each value of i, the collection of all n channel tap terms (the hs) must be pre-multiplied by a phase shift before the CZT is taken. Also, an additional step for the phase shift to combine frames is necessary. Obviously, processing is more efficient if there is no gap between frames (that is, $N_F = 1$). The term N_A can be varied to change the valid velocity range and correct for Doppler ambiguity. Doppler ambiguity correction is considered in the simulation section.

V. Simulations

Simulations were performed in two dimensions for three illuminators, two targets, and one receiver, as shown in Figure 2. The receiver was located at $(0, 0)$, the illuminators were at $(12\,\mathrm{km}, 16\,\mathrm{km})$, $(-12\,\mathrm{km}, 6\,\mathrm{km})$, and $(14\,\mathrm{km}, -14\,\mathrm{km})$, and the initial target locations were at $(12.5\,\mathrm{km}, 2.5\,\mathrm{km})$ and $(12.4\,\mathrm{km}, 2\,\mathrm{km})$. The targets moved at constant velocities of $(-175\,\mathrm{m/s}, 50\,\mathrm{m/s})$ and $(-175\,\mathrm{m/s}, 75\,\mathrm{m/s})$, respectively. Each target consisted of a five-point scatterer. Relative to the target location, the scatterers for both targets were offset by $(10\,\mathrm{m}, 0\,\mathrm{m})$, $(0\,\mathrm{m}, 10\,\mathrm{m})$, $(0\,\mathrm{m}, -10\,\mathrm{m})$, $(-10\,\mathrm{m}, 5\,\mathrm{m})$, $(-10\,\mathrm{m}, -5\,\mathrm{m})$, which is the scenario used in [5]. When

discussing the baseband signal to noise ratio (SNR) at the receiver in the following scenarios, the average power not counting the effects of Doppler was used. The transmitted data was quadrature phase-shift key (QPSK) modulated.

The complex amplitudes A_p of the target returns were chosen such that if the returns from the individual scatterers were to add coherently, the desired average SNR of the targets would be obtained. However, each scatterer was assigned a complex phase shift that was kept constant. The received signal was simulated for every single sample using the full model of Section II-B. The zero-Doppler signals were removed from the channel-tap estimates by subtracting the projection of the channel taps onto the zero-Doppler vector.

A. Scenario 1

Elementary Period	T_0	$7/64\ \mu$s
Subcarrier Spacing	$(\Delta f)^{-1}$	$8192\,T_0$
Number of Subcarriers	N	6816
Blocks Per Frame	N_B	68
Symbol Duration	T_s	$8192\,T_0$
Cyclic Prefix Duration	T_{cp}	$2048\,T_0$
Block Duration	T_b	$10240\,T_0$
NULL Symbol Duration	T_{NULL}	$0\,T_0$
Frame Duration	T_f	$696320\,T_0$

TABLE II: Parameters for the 8 MHz mode at the 8 kHz rate with a $1/4$ guard interval in the DVB standard [11]. These values are used in Scenario 1.

The first scenario considered used parameters representative of the DVB standard, which are provided in Table II. The symbols were randomly selected omitting the pilot tones that are a part of the DVB standard. The center carrier frequency was chosen to be 177.5 MHz, which is an unrealistically low carrier frequency for this standard. This carrier frequency assures that all targets were well resolved in Doppler. The second simulation scenario uses a realistic center carrier frequency, where Doppler ambiguity becomes a problem. The SNR of each of the direct-path signals from the transmitters was 20 dB above the noise floor, meaning that, in practice, the radio signals could be assumed to have been decoded without error. The target returns were 50 dB below the direct path signals. In the matched filters, all of the blocks within an OFDM frame were coherently match filtered, and the results were subsequently non-coherently combined (the squared magnitudes were added) between frames. Ten frames were combined, corresponding to a long integration period of 0.7616 s.

The results are shown in Figure 3. All six tracks from each target-illuminator pair can be resolved using the time-shift model. However, in the phase-shift model, the lack of compensation for the target motion prevents the two tracks in the upper left from being resolved. The range-migration correction came at a price. Without any particular optimization, the time-shift model implemented using the FFT and chirp-z transforms took about 13 times as long to execute as the basic matched filtering. That said, computing all of the sums by brute force took approximately 116 times as long as the basic matched filtering, indicating that the method presented in this paper offers almost a 9-fold speed improvement over the brute-force approach. Additional optimizations could improve this further.

B. Scenario 2

The third scenario is the same as the second, except a more realistic carrier frequency of 474 MHz was used. At this carrier, Doppler aliasing is present and due to the aliasing, the processing associated with the time-shift model actually results in a "tearing" effect in range for the aliased targets instead of properly eliminating the range migration, as illustrated in Figure 4b. On the other hand, if the ambiguity order is known or can be determined from other information (the correct range of velocities to choose by varying N_A from Section IV-B), then proper compensation can be performed, and the targets can once again be resolved, as illustrated in Figure 4c.

VI. Conclusion

A new time-shift model for signal processing using OFDM waveforms was introduced. The efficient implementation of matched filters for the time-shift model using a chirp-z transform and an FFT were considered. It was demonstrated that the time-shift model can reduce smearing in the range dimension of range-Doppler plots when the targets move significantly compared to the range resolution of the radar. Additionally, since the time-shift model actually worsens the smearing in the presence of Doppler ambiguity when viewing the wrong range-rate interval, but improves it when in the correct interval, it is possible that Doppler ambiguity can be resolved by choosing the highest peak across ambiguity regions.

References

[1] *ATSC Digital Television Standard Part 2 – RF/Transmission System Characteristics*, Advanced Television Systems Committee Std. A/53, Part 2:2007, Jan. 2007.

[2] M. R. Allen, S. L. Katz, and H. Urkowitz, "Geometric aspects of long-term noncoherent integration," *IEEE Transactions on Aerospace and Electronic Systems*, vol. 25, no. 5, pp. 689–700, Sep. 1989.

[3] *Transmission System for Digital Terrestrial Television Broadcasting*, Association of Radio Industries and Businesses Std. ARIB STD-B31, Rev. 1.6-E2, Nov. 2005, English Translation.

[4] M. K. Baczyk and M. Malanowski, "Decoding and reconstruction of reference DVB-T signal in passive radar systems," in *Proceedings of the 11th International Radar Symposium*, Vilnius, Lithuania, 16–18 Jun. 2010, pp. 1–4.

[5] C. R. Berger, B. Demissie, J. Heckenbach, P. Willett, and S. Zhou, "Signal processing for passive radar using OFDM waveforms," *IEEE Transactions on Signal Processing*, vol. 4, no. 1, pp. 226–238, 2010.

[6] J. W. Betz, "Effects of uncompensated relative time companding on a broad-band cross correlator," *IEEE Transactions on Acoustics, Speech, and Signal Processing*, vol. ASSP-33, no. 3, pp. 505–510, Jun. 1985.

[7] J. M. Christiansen, "DVB-T based passive bistatic radar," Master's thesis, Norwegian University of Science and Technology, Trondheim, Norway, Jun. 2009.

[8] F. Deudon, F. Le Chevalier, S. Bidon, O. Besson, and L. Savy, "A migrating target indicator for wideband radar," in *Proceedings of the IEEE Sensor Array and Multichannel Signal Processing Workshop*, Jerusalem, Israel, 4–7 Oct. 2010, pp. 249–252.

[9] *Radio Broadcasting Systems; Digital Audio Broadcasting (DAB) to Mobile, Portable and Fixed Receivers*, European Telecommunications Standards Institute Std. ETSI EN 300 401, Rev. 1.4.1, Jan. 2006.

[10] *Digital Video Broadcasting (DVB); Frame structure channel coding and modulation for a second generation digital terrestrial television broadcasting system (DVB-T2)*, European Telecommunications Standards Institute Std. ETSI EN 302 755, Rev. 1.1.1, Sep. 2009.

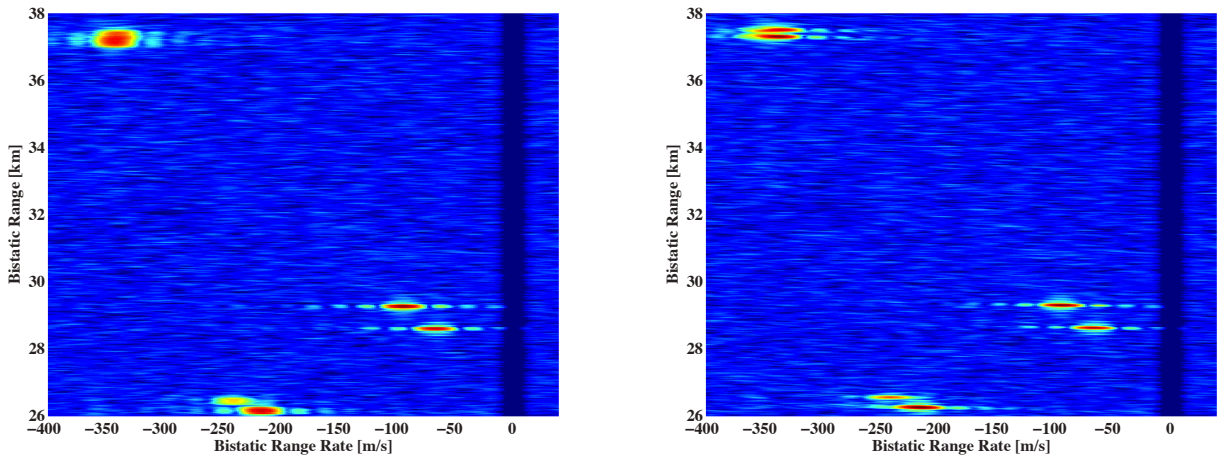

(a) The Phase-Shift Model

(b) The Time-Shift Model

Fig. 3: The delay-Doppler plots from the matched filters using each model for Scenario 2. The color scales are identical in both images. The time-shift model successfully resolves the two returns in the upper left.

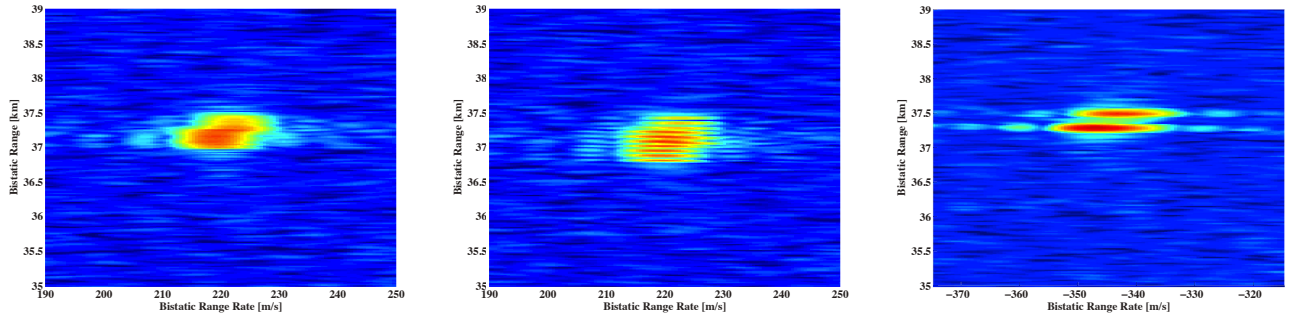

(a) The Aliased Phase-Shift Model

(b) The Aliased Time-Shift Model

(c) The Dealiased Time-Shift Model

Fig. 4: In (a) and (b) are delay-Doppler plots from the matched filters using each models for the third scenario without correcting for Doppler ambiguity. In (c), the correct ambiguity order ($N_A = 1/2$) is chosen. The color scales are identical in all three images. As a result, the tracks can again be resolved in range.

[11] *Digital Video Broadcasting (DVB); Framing structure, channel coding and modulation for digital terrestrial television*, European Telecommunications Standards Institute Std. ETSI EN 300 744, Rev. 1.6.1, Sep. 2009.

[12] G. Franken, H. Nikookar, and P. van Genderen, "Doppler tolerance of OFDM-coded radar signals," in *Proceedings of the 3rd European Radar Conference*, Manchester, UK, 13–15 Sep. 2006, pp. 108–111.

[13] S. S. Hsiao and P. G. Grieve, "Moving target detection through range cell migration radar," U.S. Patent 5,235,338, Aug. 10, 1993.

[14] *HD Radio™ FM Transmission System Specifications*, iBiquity Digital Corporation Std., Rev. E, Jan. 2008.

[15] *IEEE Standard for Local and Metropolitan Area Networks Part 16: Air Interface for Broadband Wireless Access Systems*, The Institute of Electrical and Electronics Engineers, Inc. Std. IEEE Std 802.16™-2009, May 2009.

[16] R. Lanari, "A new method for the compensation of the SAR range cell migration based on the chirp z-transform," *IEEE Transactions on Geoscience and Remote Sensing*, vol. 33, no. 5, pp. 1296–1299, Sep. 1995.

[17] F. Le Chevalier, *Principles of Radar and Sonar Processing*. Boston: Artech House, 2002.

[18] G. Lellouch and H. Nikookar, "On the capability of a radar network to support communications," in *Proceedings of the 14th IEEE Symposium on Communications and Vehicular Technology in the Benelux*, Delft, Netherlands, 15 Nov. 2007, pp. 1–5.

[19] N. Levanon, "Multifrequency complementary phase-coded radar signal," *IEE Proceedings – Radar, Sonar and Navigation*, vol. 147, no. 6, pp. 276–284, Dec. 2000.

[20] M. Malanowski and K. Kulpa, "Analysis of integration gain in passive radar," in *Proceedings of the International Conference on Radar*, Adelaide, Australia, 2–5Sep. 2008, pp. 323–328.

[21] D. V. B. Project. (2011, Aug.) DTT deployment data. [Online]. Available: http://www.dvb.org/about_dvb/dvb_worldwide/DTT-deployment-2011-08-15.xls

[22] L. R. Rabiner, R. W. Shafer, and C. M. Rader, "The chirp z transform algorithm," *IEEE Transactions on Audio and Electroacoustics*, vol. AU-17, no. 2, pp. 86–92, 1969.

[23] J. Song, Z. Yang, L. Yang, k. Gong, C. Pan, J. Wang, and Y. Wu, "Technical review on Chinese digital television broadcasting standard and measurements on some working modes," *IEEE Transactions on Broadcasting*, vol. 53, no. 1, pp. 1–7, Mar. 2007.

[24] C. Sturm, T. Zwick, and W. Wiesbeck, "An OFDM system concept for joint radar and communications operations," in *Proceedings of the IEEE Vehicular Technology Conference*, Barcelona, Spain, 26–29 Apr. 2009, pp. 1–5.

[25] (2010, May) WiMAX forum ® industry research report. WiMAX Forum. [Online]. Available: http://wimaxforum.org/files/industry_reports/Monthly_Industry_Report_May2011.pdf

[26] (2010, Sep.) Global broadcasting update: DAB/DAB+/DMB. WorldDMB. [Online]. Available: http://www.worlddab.org/rsc_brochure/lowres/12/rsc_brochure_lowres_20100910.pdf